Supplementary Information for

Enhanced energy-storage in lead-free multilayer capacitors via entropy-assisted polymorphic domain engineering

Jiaqi Li [1,2,#], Yibing Zhang [1,#], Zhen Liu [2,*], Lingling Wei [3], Haonan Peng [2], Minghao Liu [2], Shiguang Yan [2], Kunyu Zhao [2], Huarong Zeng [2,*], Zupei Yang [1,*], Genshui Wang [2,4,*]

[1] School of Material Science and Engineering, Shaanxi Normal University, Xi'an, China.

[2] Key Laboratory of Inorganic Functional Materials and Devices, Shanghai Institute of Ceramics, Chinese Academy of Sciences, Shanghai, China.

[3] School of Chemistry and Chemical Engineering, Shaanxi Normal University, Xi'an, China.

[4] The State Key Laboratory of High Performance Ceramics and Superfine Microstructure, Shanghai Institute of Ceramics, Chinese Academy of Sciences, Shanghai, China.

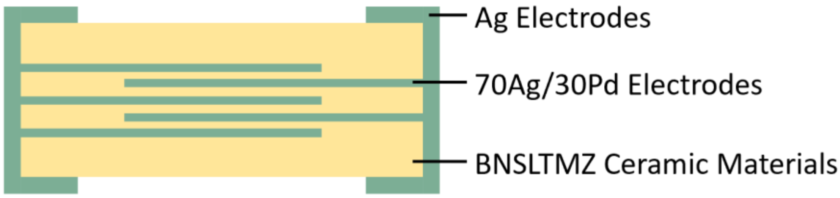

Fig. S1 The schematic diagram of the BNSLTMZ MLCCs.

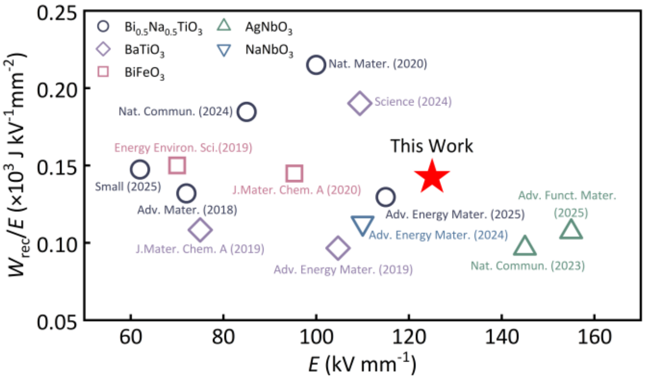

Fig. S2 The comparison of the normalized energy storage density of BNSLTMZ MLCCs with those of other recently reported state-of-the-art MLCCs.

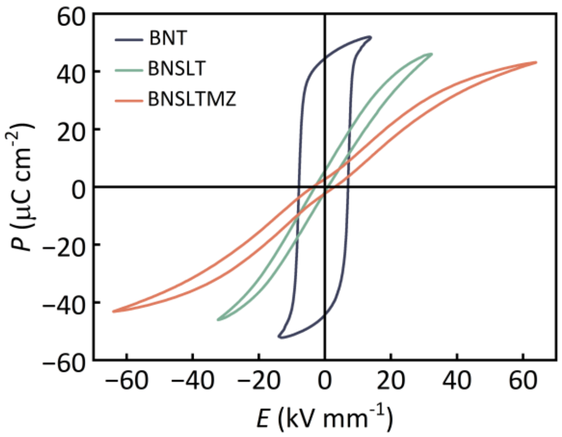

Fig. S3 Bipolar P-E loops of the BNT, BNSLT, and BNSLTMZ ceramics.

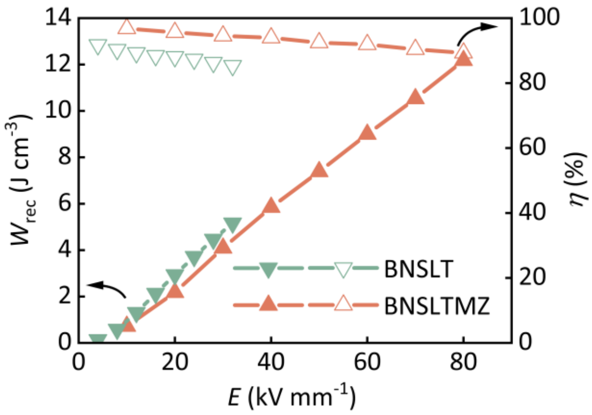

Fig. S4 W_{rec} and η of the BNSLT and BNSLTMZ ceramics as a function of applied E.

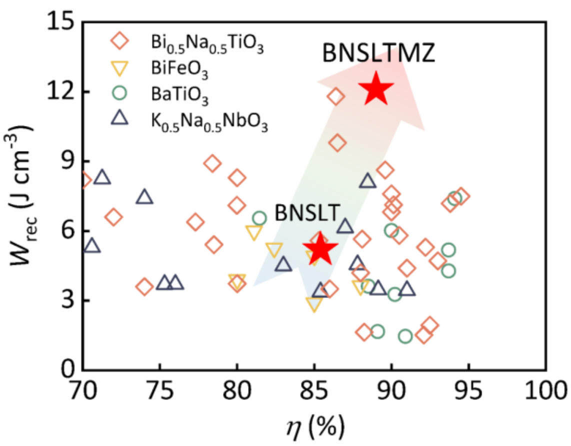

Fig. S5 The comparison of W_{rec} and η values of BNSLTMZ ceramics with those of other recently reported lead-free bulk ceramics[1-24].

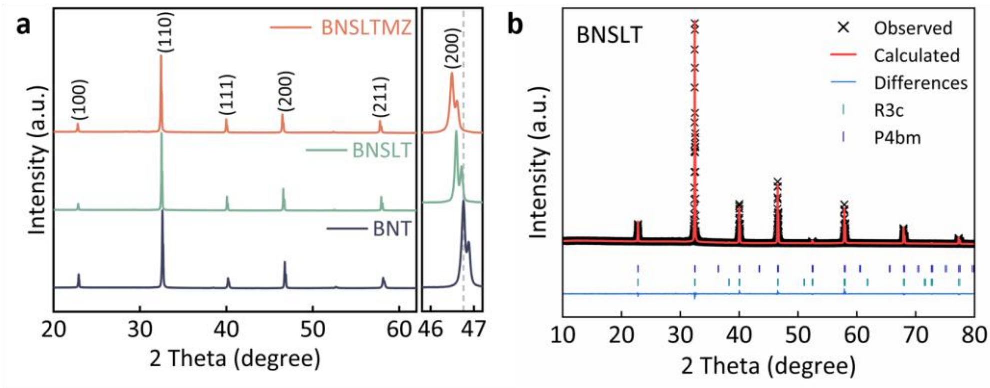

Fig. S6 a X-ray diffract (XRD) patterns of the BNT, BNSLT, and BNSLTMZ ceramics. **b** Rietveld refined XRD results of the BNSLT ceramic. All samples exhibited a pure perovskite phase, the splitting of peaks was caused by the $K_{\alpha 2}$. The (200) plane diffraction peaks shifted to lower angles, indicating increased interplanar spacing in the ceramic crystals. This was due to the larger ionic radii of the doped elements (Sr^{2+} 1.44 Å, CN=12; Mg^{2+} 0.73 Å, CN=6; Zr^{4+} 0.72 Å, CN=6), in contrast to those of the BNT components (Bi^{3+} 1.36, CN=12; Na^{+} 1.39 Å, CN=12; Ti^{4+} 0.61 Å, CN=6).

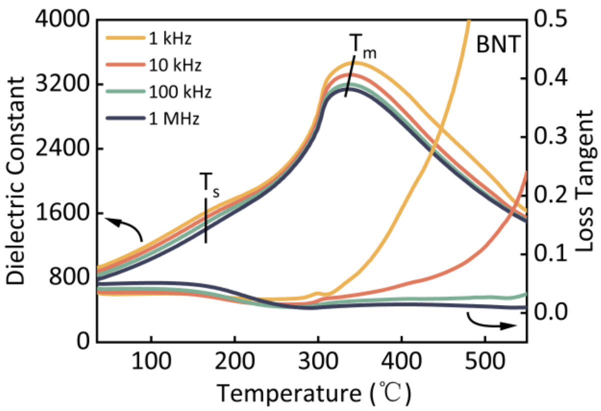

Fig. S7 Temperature-dependent dielectric constant and loss tangent of the as-sintered BNT ceramics under various frequencies from 1 kHz to 1 MHz.

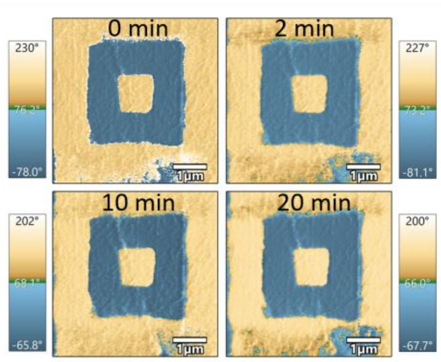

Fig. S8 Out-of-plane PFM phase pictures and domain evolution after different time for the BNT ceramics under the field of 20 V.

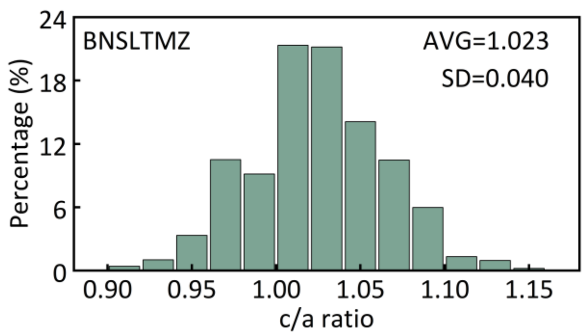

Fig. S9 Statistical c/a ratio distribution for the BNSLTMZ ceramic.

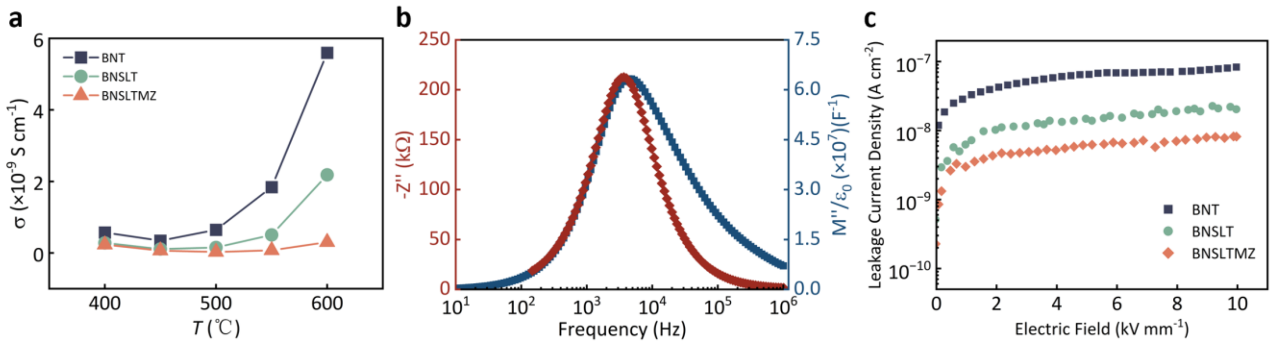

Fig. S10 **a** Variation of conductivity with temperature of BNT, BNSLT, and BNSLTMZ ceramics. **b** Spectroscopic plots of Z″ and M″ spectra at 600°C for the BNSLTMZ ceramics. **c** Leakage current densities of BNT, BNSLT, and BNSLTMZ ceramics as a function of electric field.

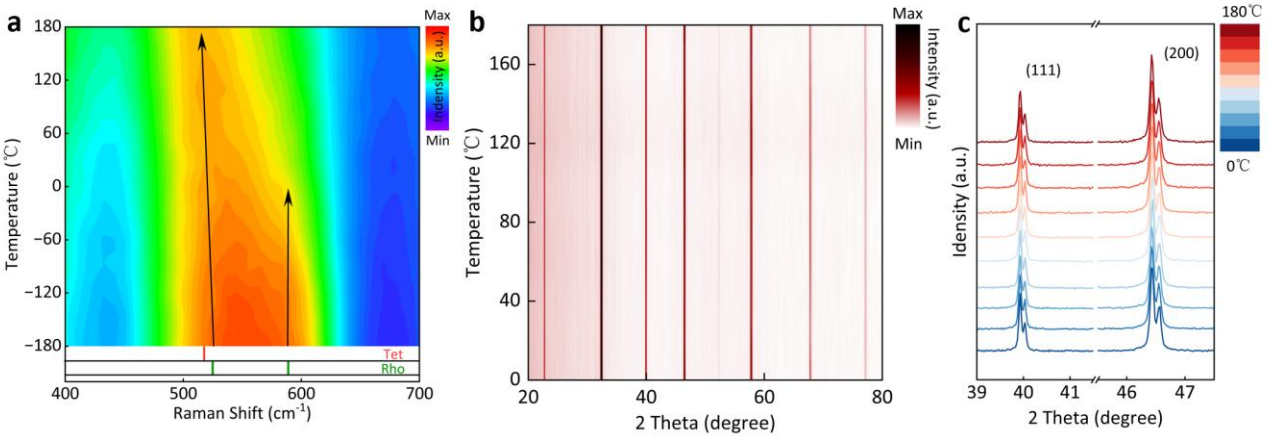

Fig. S11 a Local magnification of temperature-dependent Raman spectra between 400-700 cm^{-1} for BNSLTMZ ceramics. **b** Temperature-dependent XRD patterns of the BNSLTMZ ceramics. **c** Enlarged views of (111) and (200) peaks of **b**.

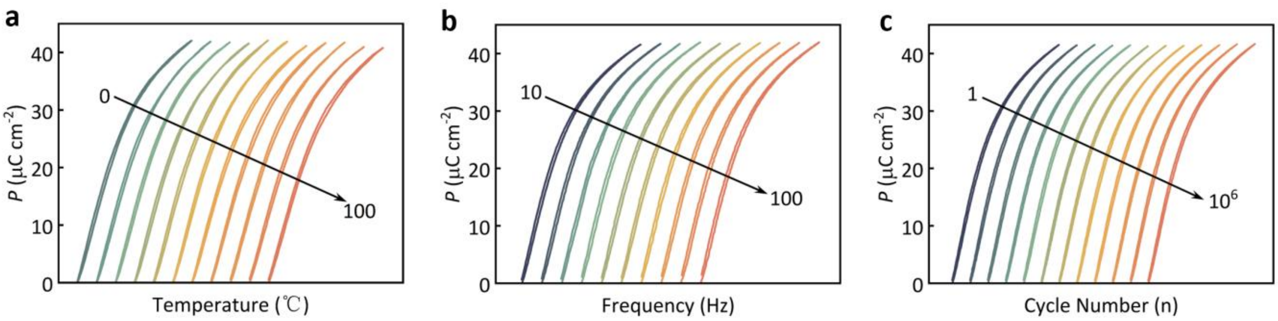

Fig. S12 a Temperature- **b** frequency- and **c** cycling-dependent *P*-*E* loops of the MLCCs.

Tab. S1 The abbreviation and general formula of the studied compositions.

Abbreviation	General Formula
BNT	$(Bi_{0.5}Na_{0.5})TiO_3$
BNSLT	$0.6(Bi_{0.5}Na_{0.5})TiO_3$-$0.4(Sr_{0.7}La_{0.2})TiO_3$
BNSLTMZ	$0.925(0.6(Bi_{0.5}Na_{0.5})TiO_3$-$0.4(Sr_{0.7}La_{0.2})TiO_3)$-$0.075Bi_{0.5}(Mg_{0.5}Zr_{0.5})O_3$

Tab. S2 Refined lattice parameters of the BNT, BNSLT, and BNSLTMZ ceramics by Rietveld method.

Ceramic abbreviation	Space group	Lattice parameters *a* (Å) *b* (Å) *c* (Å)	Content (%)	R_{wp} (%)	χ^2
BNT	*R3c*	5.489 5.489 6.753 $\alpha=\beta=90°$ $\gamma=120°$	100 [25]		
BNSLT	*R3c*	5.517 5.517 6.753 $\alpha=\beta=90°$ $\gamma=120°$	32.08	3.10	3.24
	P4bm	5.515 5.515 3.901 $\alpha=\beta=\gamma=90°$	67.92		
BNSLTMZ	*R3c*	5.532 5.532 6.753 $\alpha=\beta=90°$ $\gamma=120°$	15.54	3.09	3.32
	P4bm	5.528 5.528 3.911 $\alpha=\beta=\gamma=90°$	84.46		

References

1. Chai, Q. et al. Superior energy storage properties and optical transparency in $K_{0.5}Na_{0.5}NbO_3$-based dielectric ceramics via multiple synergistic strategies. *Small* **19**, 2207464 (2023).

2. Chen, B. et al. Influence of milling speed of high energy mechanochemical technique on microstructure and electrical properties of $K_{0.5}Na_{0.5}NbO_3$ ceramics. *J. Mater. Sci-Mater. El.* **35**, 50 (2024).

3. Wang, M., Xie, A., Fu, J., Zuo, R. Energy storage properties under moderate electric fields in $BiFeO_3$-based lead-free relaxor ferroelectric ceramics. *Chem. Eng. J.* **440**, 135789 (2022).

4. Huang, X. et al. Enhanced energy storage properties of $Bi(Ni_{1/2}Zr_{1/2})O_3$-modified $BaTiO_3$-based ceramics. *J. Mater. Sci-Mater. El.* **34**, 201 (2023).

5. Bai, M. et al. High-performance energy storage in $BaTiO_3$-based oxide ceramics achieved by high-entropy engineering. *J. Alloys. Compd.* **970**, 172671 (2024).

6. Peng, X. et al. Lead-free KNN-based ceramics incorporated with $Bi(Zn_{2/3}Nb_{1/3})O_3$ possessing excellent optical transmittance and superior energy storage density. *Mater. Res. Bull.* **165**, 112294 (2023).

7. Wang, M. et al. Significantly improved energy storage performances of $K_{0.5}Na_{0.5}NbO_3$ lead-free ceramics via a composition optimization strategy. *Inorg. Chem. Front.* **10**, 4578-4586 (2023).

8. Wang, T. et al. Synergistic enhanced energy storage performance of NBT-KBT ceramics by $K_{0.5}Na_{0.5}NbO_3$ composition design. *J. Alloys. Compd.* **948**, 169725 (2023).

9. Wu C. et al. A co-doping strategy to achieve high energy storage performance in $BiFeO_3$-based ceramics. *Ceram. Int.* **49**, 29218-29228 (2023).

10. Yang, L. et al. The enhancement of energy storage performance of $BaTiO_3$-$Bi(Mg_{0.5}Ti_{0.5})O_3$ Pb-free ceramics via an optimized viscous polymer process route. *Ceram. Int.* **50**, 14385-14396 (2024).

11. Ge, P-Z. et al. Excellent energy storage properties realized in novel $BaTiO_3$-based lead-free ceramics by regulating relaxation behavior. *J. Materiomics* **9**, 910-919 (2023).

12. Lin, L. et al. Multi-objective collaborative design optimized highly efficient energy capacitive lead-free relaxor ferroelectrics. *J. Mater. Chem. A* **11**, 21948-21958 (2023).

13. Wang, Z. et al. Ultrahigh energy-storage capacity achieved in $(Bi_{0.5}Na_{0.5})TiO_3$-based high-entropy dielectric capacitors with linear-like polarization response. *Chem. Eng. J.* **474**, 145506 (2023).

14. Wang, C., Cao, W., Liang, C., Zhao, H., Wang, C. Equimolar high-entropy for excellent energy storage performance in $Bi_{0.5}Na_{0.5}TiO_3$-based ceramics. *Energy Storage Mater.* **70**, 103534 (2024).

15. Zhao, H. et al. Suppressing interfacial polarization via entropy increase strategy for superior energy-storage performance of $Na_{0.5}Bi_{0.5}TiO_3$-based ceramics. *J. Materiomics* **10**, 947-955 (2024).

16. Chen, X. et al. Co-regulation of phase-domain structure in $Bi_{0.5}Na_{0.5}TiO_3$- based ferroelectrics to optimize energy storage properties. *Ceram. Int.* **49**, 37720-37728 (2023).

17. Tang, L. et al. Giant Energy Storage Density with Antiferroelectric-Like Properties in BNT-Based Ceramics via Phase Structure Engineering. *Small* **19**, 2302346 (2023).

18. Shi, W. et al. Moderate Fields, Maximum Potential: Achieving High Records with Temperature-Stable Energy Storage in Lead-Free BNT-Based Ceramics. *Nano-Micro Lett* **16**, 91 (2024).

19. Cao, W. et al. Boosting energy-storage performance in lead-free ceramics via polyphase engineering in the superparaelectric state. *Composites, Part B* **255**, 110630 (2023).

20. Deng, T, Liu Z, Hu, T, Dai, K, Hu, Z, Wang, G. Excellent energy-storage performance in $Bi_{0.5}Na_{0.5}TiO_3$-based lead-free composite ceramics via introducing pyrochlore phase $Sm_2Ti_2O_7$. *Chem Eng J* **465**, 142992 (2023).

21. Li, X. et al. Enhanced high-temperature energy storage properties in BNT-based ceramics with well-controlled low dielectric loss. *Ceram. Int.* **50**, 1438-1442 (2024).

22. Lin, L, Li, C, Liu, J, Bai, W, Li, W, Zhai, J. Boosting capacitive performance of lead-free relaxor ferroelectrics by introducing a linear dielectric. *Ceram. Int.* **50**, 829-837 (2024).

23. Guo, J. et al. Multi-symmetry high-entropy relaxor ferroelectric with giant capacitive energy storage. *Nano Energy* **112**, 108458 (2023).

24. Xi, J. et al. Polymorphic Heterogeneous Polar Structure Enabled Superior Capacitive Energy Storage in Lead-Free Relaxor Ferroelectrics at Low Electric Field. *Small* **20**, 2400686 (2024).

25. Jones GO, Thomas PA. Investigation of the structure and phase transitions in the novel A-site substituted distorted perovskite compound $Na_{0.5}Bi_{0.5}TiO_3$. *Acta Crystallographica Section B* **58**, 168-178 (2002).